Electronic Supplementary Information (ESI)
Palladium dispersion effects on wet methane oxidation kinetics

Peter Velin[a], Carl-Robert Florén[a], Magnus Skoglundh[a], Agnes Raj[b], David Thompsett[b], Gudmund Smedler[c] and Per-Anders Carlsson[a,*]

[a]Department of Chemistry and Chemical Engineering, Competence Centre for Catalysis, Chalmers University of Technology, SE-41296 Göteborg, Sweden

[b]Johnson Matthey Technology Centre, Blounts Court, Sonning Common, Reading, RG4 9NH, UK

[c]Johnson Matthey AB, 421 31, Västra Frölunda, Sweden

July 9, 2020

Lay-out of the ESI

This ESI document contains a presentation and brief discussion of mass and heat transport effects in the experiments (section 1), multiscale simulations (section 2) and additional data (section 3) that includes complete data sets and a few complementary measurements/data sets presented as tables and figures. The figures lay-out of the figures are analogous to those in the main document.

1. Mass and heat transport effects

Here the mass and heat transport effects on the reaction rate are evaluated for a methane conversion of 25%, which exceeds the maximum conversion of 15% used for kinetic data analysis. For a powder catalysts, possible external mass transfer limitations can be checked for by comparing the difference in methane concentration between the bulk gas and catalyst grain (ΔC_{CH_4}) with the bulk gas concentration of methane ($C^b_{CH_4}$). The observed reaction rate is calculated as:

$$r_{obs} = q\frac{p_{CH_4}}{RT}\frac{X}{W} \tag{1}$$

where q is the volumetric flow rate at room temperature ($3.3\cdot10^{-6}$ m^3/s), p_{CH_4} is the partial pressure of methane (10^2 Pa), R is the molar gas constant (8.31 J/(mol K), T is temperature (298.15 K), X is the methane conversion (0.25) and W is the amount of catalyst ($1.6 \cdot 10^{-4}$ kg). Substituting these values into eqn. 1 gives $r_{obs} = 1.3 \cdot 10^{-4}$ mol/(s kg catalyst). The steady-state reaction rate for a packed-bed reactor with spherical catalyst pellets (here grains) is coupled to the external mass transfer (film transport) by:

$$r = S_m k_c \Delta C_{CH_4}, \tag{2}$$

where $S_m = 6/d\rho$ is the external surface area of the grain per mass of grain and d_p and ρ_p are the grain diameter and density, respectively. The mass transfer coefficient (k_c) equals ShD/d where Sh is the Sherwood number and D the binary gas diffusivity. Eqn. 2 can be rearranged to:

$$\Delta C_{CH_4} = \frac{rd^2\rho}{6ShD} \tag{3}$$

Substituting r_{obs} for r and assuming a reasonable low value for the Sherwood number ($Sh = 1.5$) and high number for the grain diameter ($d = 150 \cdot 10^{-6}$ m^2) will produce an estimate of the largest concentration gradient. Using $\rho = 1.5 \cdot 10^3$ kg/m^3, $D = 6.1 \cdot 10^{-5}$ m^2/s results in $\Delta C_{CH_4} = 7.8 \cdot 10^{-6}$ mol/m^3, which is negligible compared to $C^b_{CH_4} = p_{CH_4}/(RT) = 0.017$ mol/m^3 at T=723 K.

The influence of internal mass transport limitations on the reaction rate in a porous catalyst grain can be checked for by using the Weisz-Prater criterion stating that for an isothermal spherical catalyst grain and a first-order reaction the Weisz modulus (Φ) should not exceed 1 for the grain to be free from rate limiting internal concentration gradients. If fulfilled, the efficiency factor (η) is high, i.e., ≥ 0.95. The appropriate expression for the Weisz modulus is [P.B. Weisz and C.D. Prater, Adv. Catal. 6 (1954) 143–196]:

$$\Phi = \frac{r_v r^2}{C^s_{CH_4} D_{eff}} \tag{4}$$

where r_v is the observed reaction rate per volume of catalyst, r is the grain radius, $C^s_{CH_4}$ is the methane concentration at the outer surface of the grain and D_{eff} is the effective diffusivity. With $r_v = r_{obs}\rho$ and as the external mass transfer is rapid, the concentration at the surface of a catalyst grain is well approximated with the methane concentration in the gas bulk eqn. 4 can be expressed as:

$$\Phi = \frac{r_{obs}\rho r^2}{C^b_{CH_4} D_{eff}} \tag{5}$$

where $r = d/2 = 75 \cdot 10^{-6}$ m^2 and $D_{eff} = 3.8 \cdot 10^{-7}$ m^2/s. This gives $\Phi \approx 0.17 < 1$ clearly indicating the absence of internal mass transport limitations.

The influence of internal heat transfer limitations can be estimated by using the Anderson criterion [J. B. Anderson, Chem. Eng. Sci. 18(2) (1963) 147–148.]

$$\frac{|\Delta H_r| r_{obs} \rho r^2}{\lambda_{eff} T^s} < 0.75 \frac{RT^s}{E} \quad (6)$$

where λ_{eff} is the effective thermal conductivity (30 W K^{-1}), T^s is the surface temperature of the catalyst grain (723 K) and E is the true activation energy ($180 \cdot 10^3$ J $mol^{-1}K^{-1}$). Satisfying the criterion implies that r_{obs} does not differ from the rate at constant temperature by more than 5%. With these values the left and right hand side of eqn. 6 equals $4.1 \cdot 10^{-8}$ and 0.025, respectively. Thus the criterion is satisfied. The large difference between the left and right hand sides of the inequality is mainly due to the small particle size.

2. Multiscale simulations

Complementary to experiments, multiscale simulations of dry and wet methane oxidation over the parent and modified monolith catalysts were performed. The methane conversion over the monolith catalysts at temperatures between 300 and 500 °C, was conceptually simulated in steps of 20 °C using a multiscale model implemented in MATLAB software (R2017®) to deliver the steady-state solutions to the differential equations by use of the ode15s function [C.-R. Florén *et al.*, Catal. Sci. Technol. 8 (2018) 508–520 and C.-R. Florén *et al.*, Catal. Sci. Technol. 9 (2019) 3055–3065] . The code includes first-principles surface kinetics and a reactor model for mass and heat transport. The surface kinetics is developed for the PdO(101) surface exposing under-coordinated palladium and oxygen atoms and uses a (3 × 1) surface unit cell with four PdO trilayers [M. Van Den Bossche *et al.*, J. Am. Chem. Soc. 137 (2015) 12035–12044]. The reactor model describes the axial and radial mass and heat transport inside a single monolith channel. The external mass transfer is based on equimolar counter diffusion whereas the internal mass transport is described by the effective diffusivity that accounts for bulk and Knudsen diffusion. Concerning heat transport, radial isothermal conditions are assumed and losses occur at the monolith ends.

The simulations underestimate the observed methane conversions in dry conditions as shown in Figure S1a. The difference, however, between the simulated and experimental extinction profiles decreases with increasing palladium loading. For the highest palladium loading of 3.6 wt.-%, the simulated profile agrees well with experiments except for temperatures below 380 °C. Below this temperature, the simulations show a steeper extinction than observed experimentally. On the contrary, for wet conditions, an opposite trend is seen, *cf.* Figure S1b. Upon adding 10 % water to the feed, the simulated methane conversions are generally higher than the corresponding experimentally observed conversions. In this case, the simulations for the 0.23PdAl catalyst show a better agreement but this is likely to be due to the generally lower activity in the experiments. The corresponding simulations for the modified samples are shown in Figure S1c and d. The simulations generally agree better with the experiments in foremost dry but also wet conditions. This can be explained by the fact that the kinetic model refers to a methane oxidation mechanism on a PdO(101) surface alone. Thus it lacks a description of PdO particles and support effects, which for the modified samples are expected to play a less important role as the PdO particles are large. Further, the low presence of PdO rim sites makes reverse spill-over of hydroxyls less of an issue in experiments with the modified catalysts such that the processes on the active PdO particles dominate the methane conversion, and these are better captured by the model.

The kinetic model includes two types of surface sites, i.e., reactive oxygen sites (S_O) and palladium sites (S_{Pd}). Mechanistically, all species adsorb on palladium sites except hydrogen that adsorbs on the reactive oxygen. From the simulations, it is straight-forward to extract the site coverage (θ) of each surface species at condi-

tions of interest as to understand what may limit the overall catalytic activity. In Figure S2 the average coverage of the most abundant surface species throughout the catalytic coating is plotted against temperature for dry (left panel) and wet (right panel) conditions for the 0.93PdAl sample. As discussed above, the methane conversion is underestimated for dry conditions and low temperatures. It is clear that for these conditions, the model predicts a considerable hydrogen coverage that effectively blocks reactive oxygen and hinders dissociation of methane. The overall methane oxidation rate thus becomes limited by the availability of reactive oxygen sites and as can be seen, the corresponding O coverage is low. It may seem that the blocking of reactive oxygen sites is exaggerated in the model. This is, however, not necessarily true. As discussed above, the kinetic model is not developed for a supported catalyst with all its richness in structural variation. It is thus more likely that the discrepancies in methane conversion can be explained by the lack of structural properties and mechanistic steps for the supported catalyst in the model. In the presence of water, the methane conversion is overestimated in the simulations. Although for these conditions, the catalyst surface contains few free palladium sites on which methane can dissociate, the discrepancy is indicative of a model that lacks the description of PdO rim sites that are sensitive to water. Thus, despite the lack of a full description of supported palladium catalyst, one may interpret the simulation results as indicative of that PdO rim sites are important for the oxidation of methane. This is in line with the experimental results showing that PdO dispersion should be high but not too high to balance palladium utilisation and water tolerance.

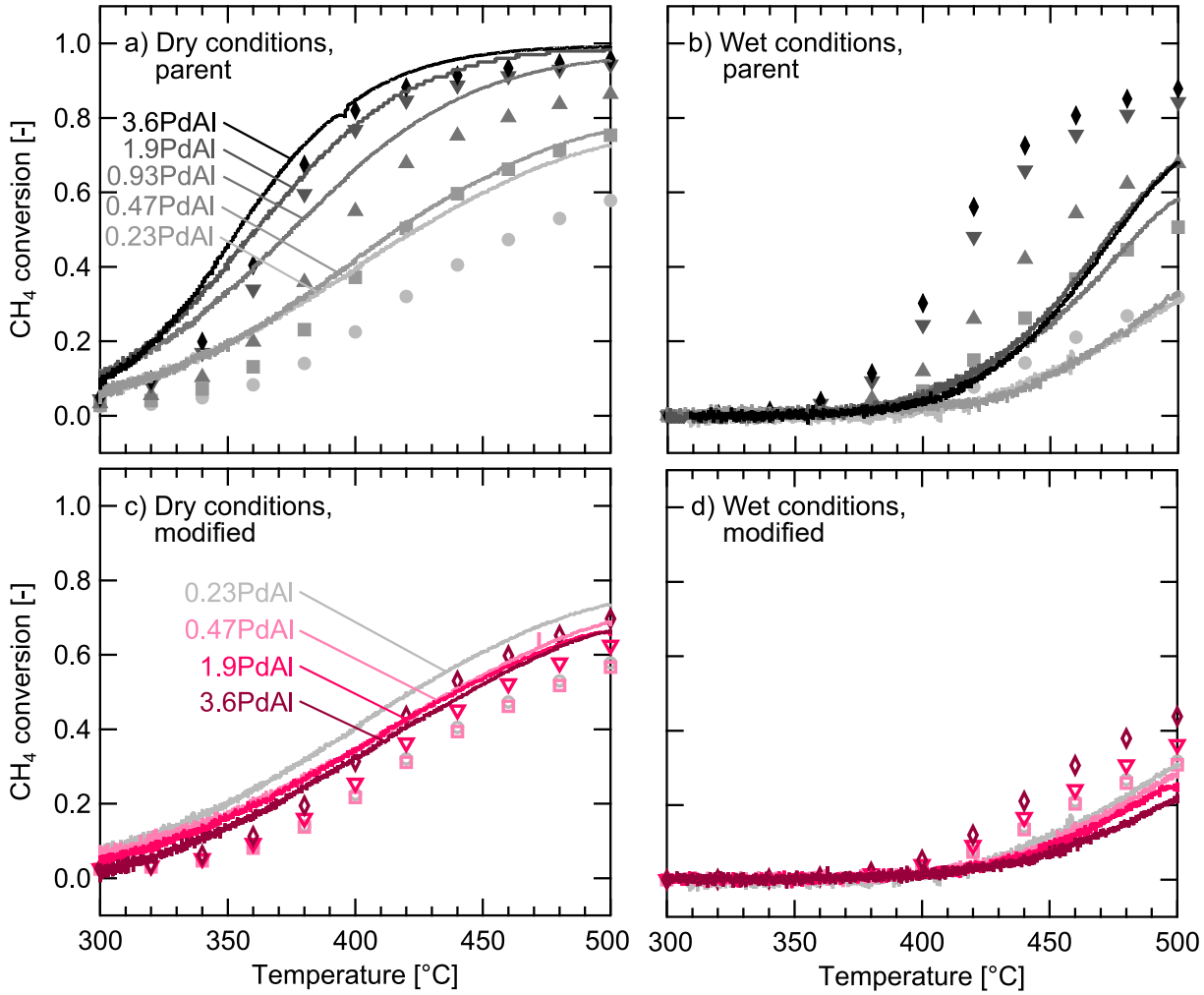

Figure S1: Experimental (solid lines) and simulated (symbols) methane oxidation extinction profiles for the parent (top panels) and thermally treated (bottom panels) Pd/Al_2O_3 monolith catalysts in dry conditions using 0.1 % CH_4 and 2 % O_2 (left panels) and wet conditions using 0.1 % CH_4, 2 % O_2 and 10 % H_2O in Ar.

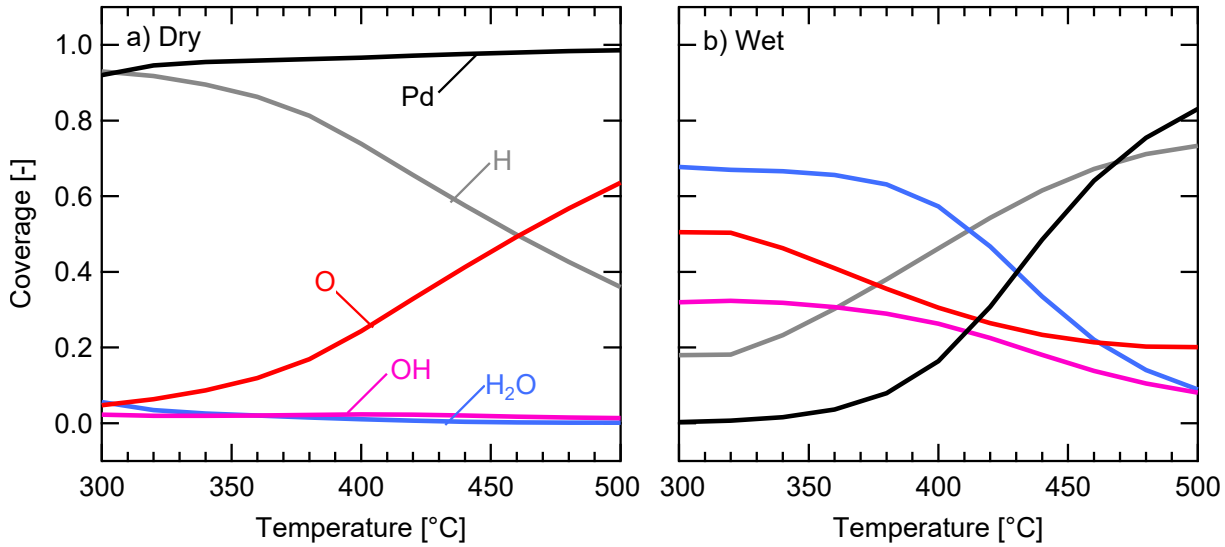

Figure S2: The coverage of hydrogen (grey), hydroxyls (purple), water (blue) and free sites of palladium (black) and oxygen (red) for the PdO surface at gas compositions of 0.1 vol% CH_4 + 2 vol% O_2 (panel a), and 0.1 vol% CH_4 + 2 vol% O_2 + 10 vol% H_2O (panel b) simulated for the 0.93PdAl sample.

3. Additional data

Table S1 summarises the CO uptake for the fresh and used powder and monolith catalysts. A significant drop in CO uptake and thus calculated palladium area is seen for the two fresh monolith samples coated with 0.23PdAl and 1.9PdAl powder as compared to the powder itself. For 0.23PdAl, the coating procedure results in a decrease from 9.7 to 4.4 μmol CO g^{-1}, and a corresponding decrease from 28 to 20 μmol CO g^{-1} for 1.9PdAl. A similar decrease is furthermore measured for all the monolith samples used in the flow reactor. The most likely explanation to this is an uneven accumulation of catalyst and binder material on the monolith during the coating procedure and possibly also that parts of the catalyst particles become blocked by the binder material. The lower palladium loadings (cf. Table S1) as compared to the powder samples support the uneven coating. The used monoliths coated with 0.23PdAl and 1.9PdAl show slightly lower CO uptake than the fresh ones. The largest decrease in CO uptake is seen for the 0.23PdAl sample, indicating that more well dispersed samples are more prone to loose active sites. However, the effect is small and should not be described as a severe sintering.

Table S2 summarises the reaction orders for wet methane oxidation over the modified powder catalysts. The reaction orders agree with previous values for palladium-alumina systems, for example the ones reported by Willis et al. [ACS Catalysis 7 (2017) 7810-7821].

Figure S3 shows STEM-HAADF images for the fresh and used monolith samples. The palladium particle diameter is approximately 7 nm ($\pm$2 nm), which indicates that no severe sintering occur during the kinetic tests.

Figure S4 shows the experimental methane oxidation extinction profiles for all powder samples exposed to dry and wet (10% water) conditions.

Figure S5 shows the experimental methane oxidation extinction profiles for all monolith samples exposed to dry and wet (10% water) conditions.

Figure S6 shows the E^* obtained from the Arrhenius curves for each parent and modified powder and monolith catalyst.

Table S1: CO uptake for fresh powders and monoliths and a three modified samples. CO uptake, Pd loading, area and dispersion for used monolith samples.

Sample ID	CO uptake (fresh powder) (μmol g^{-1})	CO uptake (fresh monolith) (μmol g^{-1})	CO uptake (used monolith) (μmol g^{-1})	Pd loading[a] (used monolith) (wt.-%)	Pd area (used monolith) (m^2 g^{-1})	Pd dispersion (used monolith) (%)
0.23PdAl	9.7	4.4	3.6	0.20	0.28	25
0.47PdAl (modified)	15 (9.6)	- (-)	6.3 (3.5)	- (-)	0.54 (0.27)	24 (12)
0.93PdAl	21	-	9.1	-	1.3	21
1.9PdAl (modified)	28 (11)	20 (-)	18 (4.0)	1.4 (-)	1.8 (0.32)	20 (3.7)
3.6PdAl (modified)	32 (13)	- (-)	22 (5.4)	- (-)	2.3 (0.41)	13 (2.4)

[a]Determined by ICP-OES

Table S2: Reaction orders with respect to CH_4 and O_2 in presence of 10% H_2O and H_2O for modified Pd/γ-Al_2O_3 catalysts at 450 °C.

Sample	CH_4	O_2	H_2O
0.23PdAl	0.65	0.25	-0.90
0.47PdAl	0.55	0.23	-0.85
0.93PdAl	0.67	0.17	-0.93
1.9PdAl	0.66	0.24	-0.92
3.6PdAl	0.77	0.23	-0.95

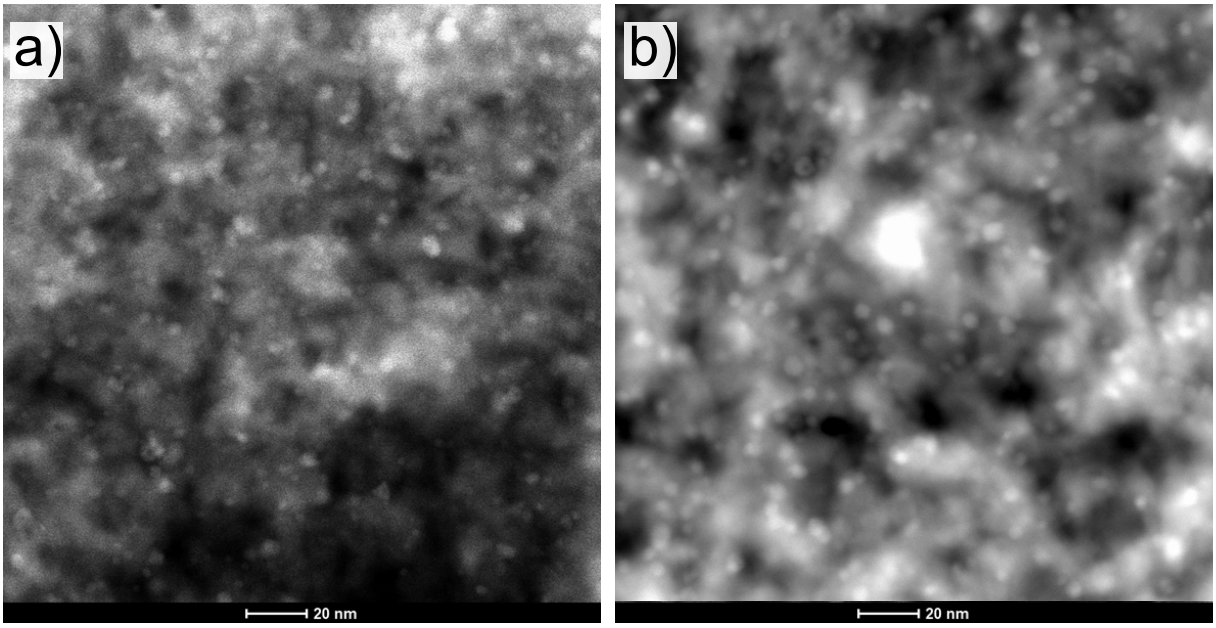

Figure S3: STEM HAADF micrographs showing PdO particles of similar size for the fresh (panel a) and used (panel b) monolith samples coated with 1.9PdAl.

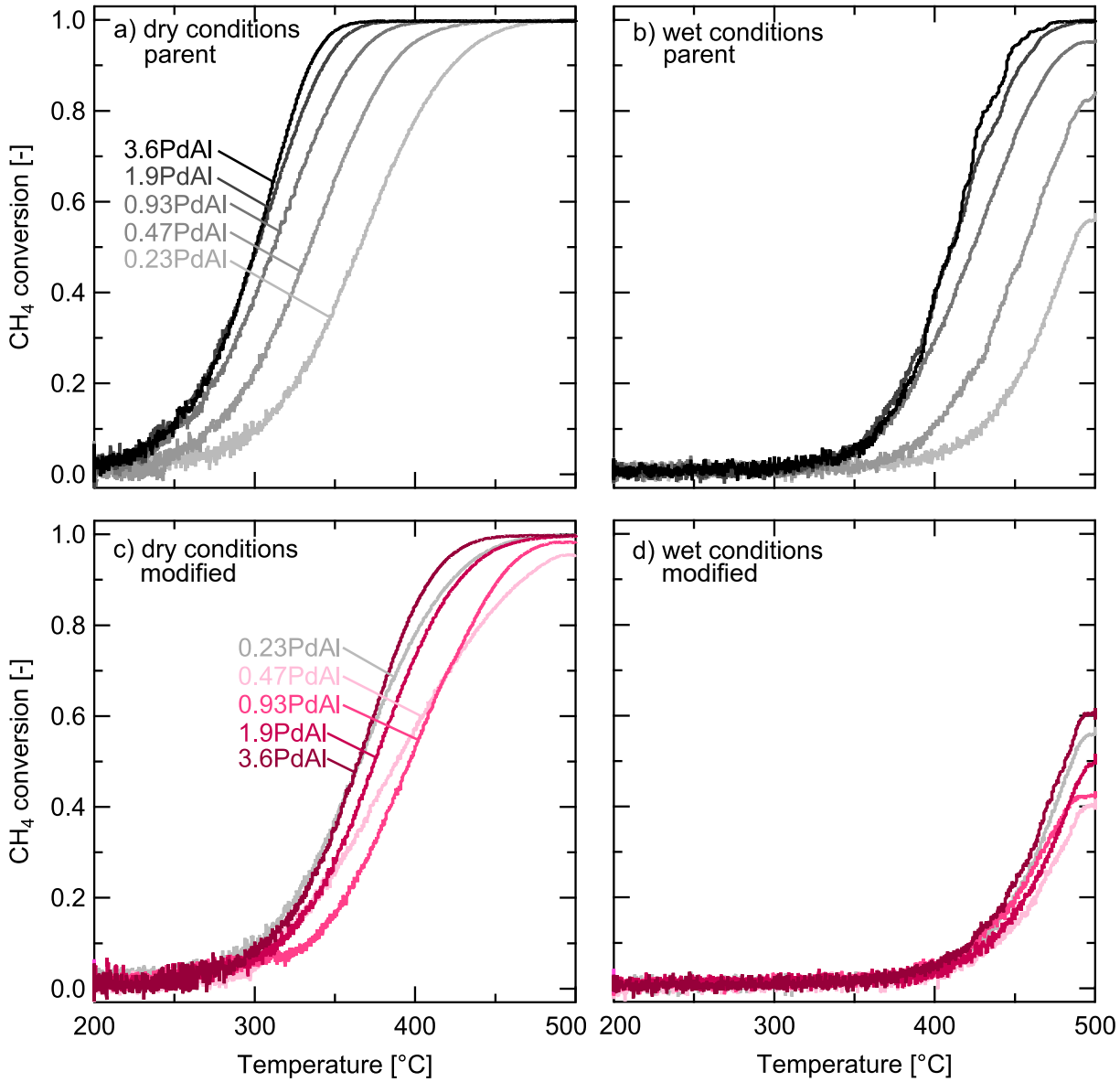

Figure S4: Experimental methane oxidation extinction profiles for 0.23, 0.47, 0.93, 1.9 and 3.6 wt.-% Pd/Al_2O_3 powder catalysts. Parent (top row) and modified samples with similar palladium areas but varied ratios of bulk-to-interface palladium sites (bottom row). Dry oxidation of 0.1 % CH_4 with 2 % O_2 (left column) and wet oxidation of 0.1 % CH_4 with 2 % O_2 in 10 % H_2O (right column).

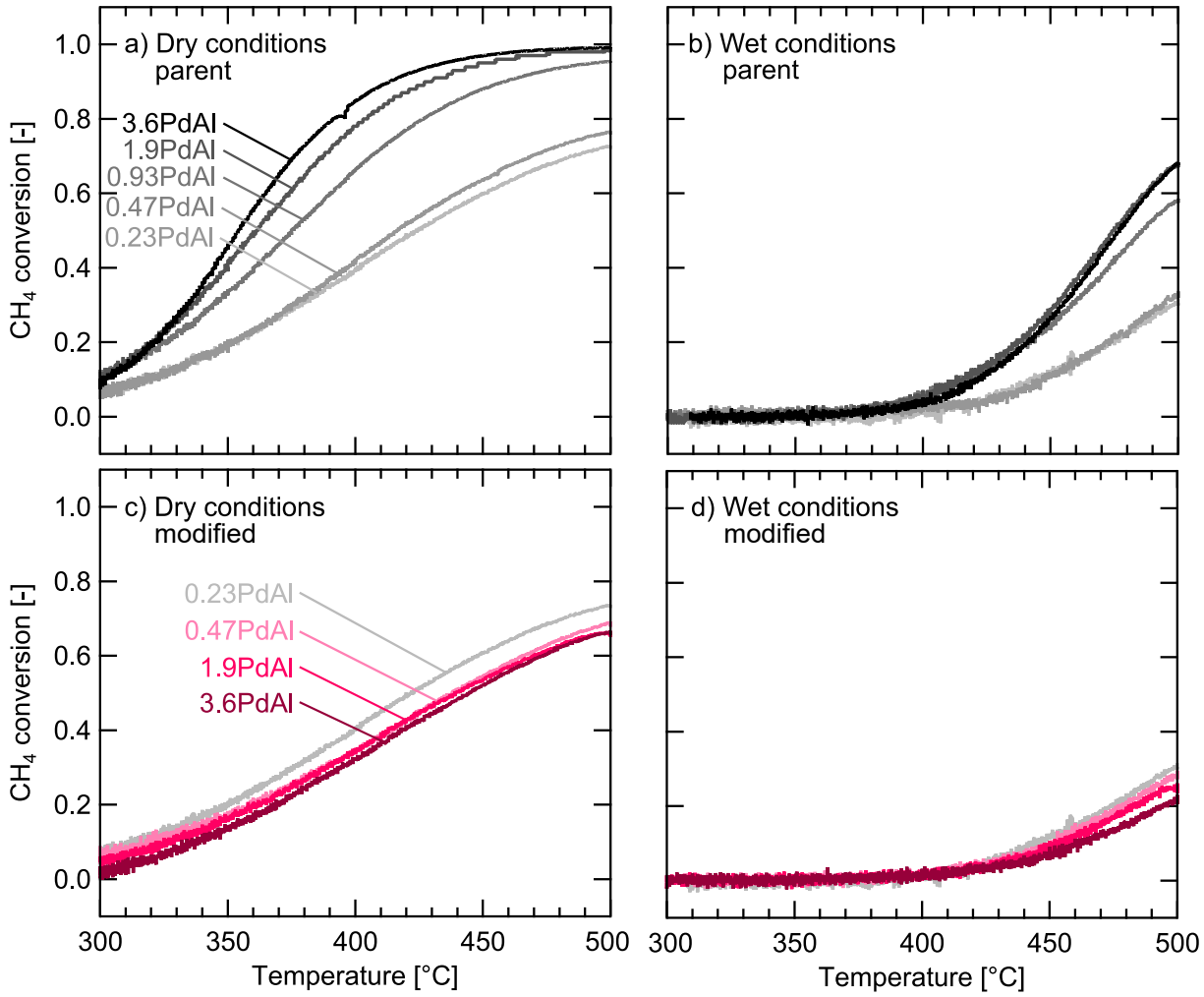

Figure S5: Experimental methane oxidation extinction profiles for 0.23, 0.47, 0.93, 1.9 and 3.6 wt.-% Pd/Al_2O_3 monolith catalysts. Parent (top row) and modified samples with similar palladium areas but varied ratios of bulk-to-interface palladium sites (bottom row). Dry oxidation of 0.1 % CH_4 with 2 % O_2 (left column) and wet oxidation of 0.1 % CH_4 with 2 % O_2 in 10 % H_2O (right column).

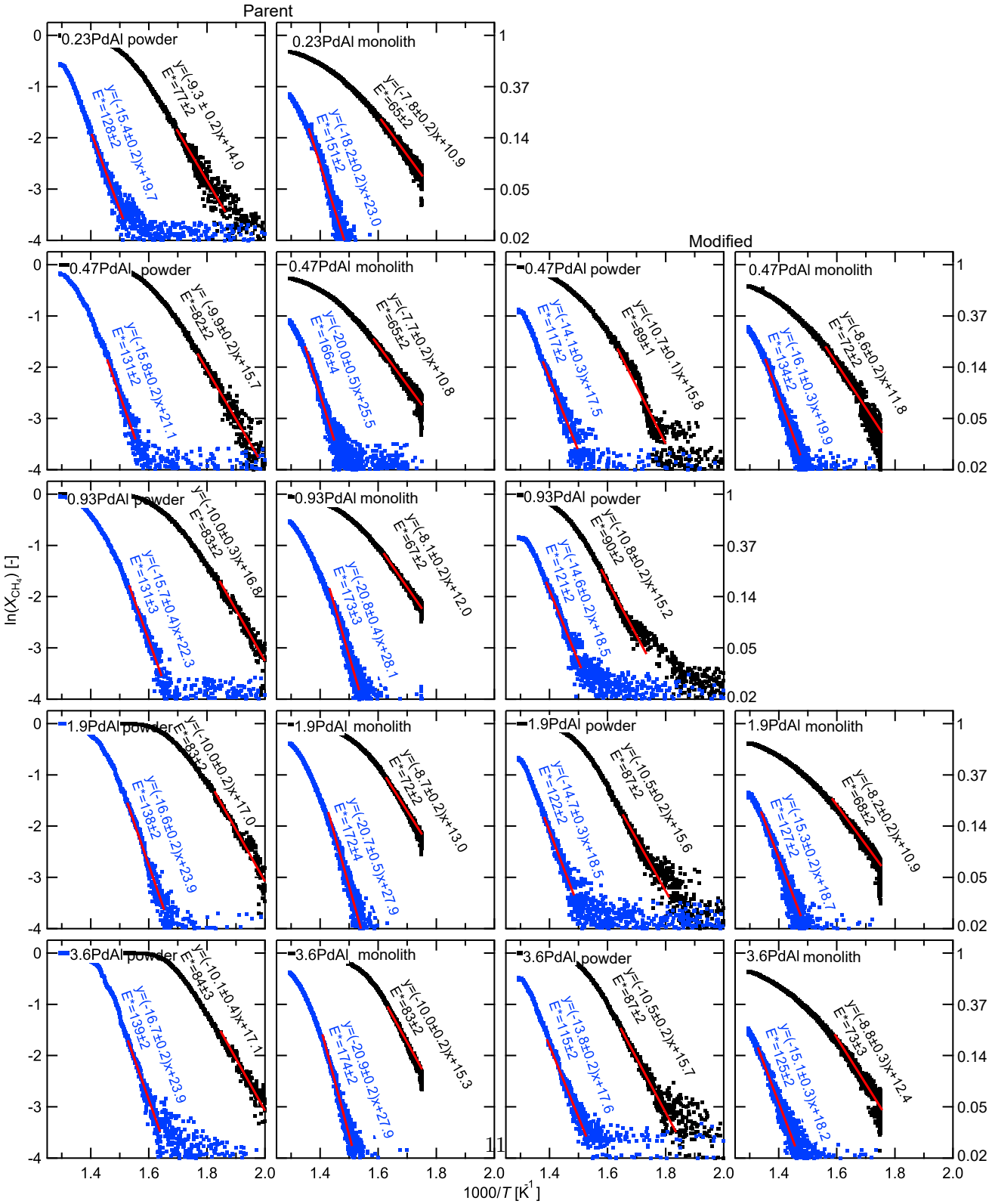

Figure S6: Arrhenius curves for the last extinction processes in dry (black) and wet (blue) conditions where red lines indicate used regression regions for the parent powder (first column), parent monolith (second column), modified powder (third column) and modified monolith (fourth column) catalysts.